VNU Journal of Science: Natural Sciences and Technology

Journal homepage: https://js.vnu.edu.vn/NST

Original Article

Synthesis of CeO_2 Coupling rGO Material Oriented to Rhodamine B Degradation under Optical Irradiation

Nguyen Hoang Hao[1,*], Nguyen Thi Ngoc Anh[1], Nguyen Duy Kien[1], Hoang Yen Nhi[1], Phan Dinh Khanh Nguyen[1], Nguyen Thi Hoa[1], Phung Thi Lan[2], Nguyen Van Thuc[3]

[1]*College of Education, Vinh University, 182 Le Duan, Vinh, Nghe An, Vietnam*

[2]*Hanoi National University of Education, 136 Xuan Thuy, Cau Giay, Hanoi, Vietnam*

[3]*VNU University of Science, 19 Le Thanh Tong, Hoan Kiem, Hanoi, Vietnam*

Received 04th April 2024
Revised 03rd July 2024; Accepted 09th July 2024

Abstract: In the present work, CeO_2 with different loading was embedded on reduced graphene oxide (rGO) by a simple one-pot hydrothermal method. The synthesized samples were characterized using XRD, EDX mapping, FESEM, and UV-Vis DRS techniques. The photocatalytic activity of the as-synthesized CeO_2, rGO, and 0,5% (1,5% and 5,0% wt) CeO_2/rGO was studied by monitoring the degradation of Rhodamine B dye (denotes RhB) under xenon light irradiation. The analyses show that CeO_2 particles were evenly dispersed on rGO and the optical properties of the xCeO_2/Rgo (x = 0,5; 1,5; and 5,0%wt)/rGO material were significantly enhanced due to the interaction between CeO_2 and rGO. The effects of CeO_2 loading, initial RhB concentration, and pH were thoroughly investigated. Under the irradiation, the RhB degradation reached 100% over 1.5%CeO_2/rGO. The high performance of the synthesized composites was attributed to the significant suppression of the recombination rate of photo-generated electron-hole pairs due to charge transfer between rGO sheets and CeO_2 particles and the smaller optical band-gap in the CeO_2/rGO nanocomposite.

Keywords: Reduced graphene oxide (rGO), CeO_2, Rhodamine B, photocatalysis.

1. Introduction

The unsuitable discharge of wastewater containing various harmful pollutants, e.g. harmful organic dyes used in the textile industry, has become a severe threat to the water environment [1]. Many techniques, including physical adsorption, photocatalysis, chemical oxidation, and nanofiltration have been used to remove dangerous pollutants from water [2, 3]. Among them, photocatalysis is thought to be a promising technique in the elimination of water due to its high efficacy, low cost, and environmental friendliness [4]. Therefore, developing highly efficient and long-lasting photocatalysts is essential to the photocatalysis process.

* Corresponding author.
E-mail address: haonguyen0404@gmail.com

https://doi.org/10.25073/2588-1140/vnunst.5658

Cerium dioxide (CeO_2), an environmentally friendly rare earth oxide, has attracted a lot of attention about its low cost, good chemical stability, good oxygen transfer capability, Ce^{3+}/Ce^{4+} redox pairs, and capacity to degrade a variety of pollutants [5, 6]. However, the usefulness of CeO_2 in photocatalysis is restricted by a broad bandgap, and CeO_2 particles tend to become agglomerated during their processing, which often leads to their poor catalyst activities [7]. Consequently, a variety of techniques have been developed to enhance light absorption, including element doping [8], noble metal deposition [9], and heterojunction structure construction [10]. Among these, developing a heterojunction with additional semiconductors has proven to be a successful technique because it can increase solar energy utilization and hasten the separation of charge carriers produced by photosynthesis [11].

The previous problems might be resolved by adhering these CeO_2 particles to reduced graphene oxide (rGO) surfaces. rGO contains functional groups like hydroxyl and epoxide groups on the basal plane and carboxyl groups at the edge [12, 13]. The presence of π-conjugation systems and oxygen groups causes rGO to absorb visible light and impart high hydrophilicity to rGO. Moreover, rGO effectively inhibits the agglomeration of CeO_2 particles and acts as electron acceptors to reduce the band gap of CeO_2. Additionally, they are also capable of resolving the critical problem of poorly ordered graphene sheet stacking brought on by π-π interactions. More active sites will be effectively exposed by a highly homogeneous distribution of CeO_2 particles on rGOs, which is crucial for catalytic performance [14-16].

2. Experimental

2.1. Chemicals

Chemicals such as H_2SO_4, $KMnO_4$, KNO_3, H_2O_2, Na_2CO_3, $Ce(NO_3)_3$, graphite, and rhodamine B were purchased from China with purity greater than 99%.

2.2. Materials Synthesis

2.2.1. Preparation of CeO_2 Material

To synthesize CeO_2, 50 mL of $Ce(NO_3)_3$ (0.05 M) was first added to 75 mL of Na_2CO_3 solution (0.075 M). The resulting solution was stirred magnetically for 30 minutes and transferred into a 200 mL Teflon flask. The Teflon flask is placed in a stainless steel flask, then placed in a drying oven for 24 hours at 200 ^oC. After natural cooling, the precipitate was washed with ethanol and separated by centrifugation at 7000 rpm several times. The obtained powder was dried at 100 ^oC in air for 10 hours.

2.2.2. Preparation of rGO Material

The rGO synthesis process follows these steps:

Step 1: Add 2 g of graphite to 100 mL of 98% H_2SO_4 while stirring for 20 minutes, then gradually add 4 g of KNO_3 and stir for 3 hours. Next, add 8 g of $KMnO_4$, stir for 4 hours, and keep the temperature below 10 ^oC. Afterward, raise the system temperature to 35 ^oC and stir for 17 hours, then add 200 mL of a 5% H_2SO_4 solution and continue stirring for 4 hours.

Step 2: Lower the temperature to room temperature, then add 25 mL of 30% H_2O_2 gradually (oxidize the remaining $KMnO_4$) and stir for 2 hours to obtain a light brown product.

Step 3: Wash and centrifuge the product in step 2 with 5% H_2SO_4, then continue washing with distilled water until pH 7. Finally, filter to remove solids and dry overnight.

2.2.3. Preparation of CeO_x/rGO Material

40 mL of rGO (10 mg/mL) was diluted with 120 mL of deionized water. Next, add V mL (calculated amount) of 0.05 M Ce^{3+} solution into 160 mL of the obtained GO solution and ultrasonicate for 30 minutes. Then, gradually add 40 mL of 0.075 M Na_2CO_3 and stir continuously for half an hour. Put the mixture in a Teflon jar and dry at 200 ^oC for 18 hours. Finally, the obtained product was washed to a neutral pH and dried at 80 ^oC for 12 hours. The as-preapred materials were denoted as x%CeO_2/r-GO (x = 0.5, 1.5, and 5.0).

2.3. Characterization Techniques

The X-ray diffraction (XRD) spectroscopy was carried out on a Bruker D8 Advance diffraction machine with a Cu-K radiation source (wavelength 0.15418 nm) to evaluate the presence of crystalline phases. The energy dispersive X-ray spectroscopy (EDX) and FeSEM images were performed on the FESEM S-4800 equipment system in Horiba, England, to determine elemental composition and the morphology of the material. The ultraviolet-visible diffuse reflectance spectrum (UV-Vis DRS spectrum) was performed on a Shimadzu UV-2600 device in Japan to determine the light absorption ability of the material.

Photocatalytic activity evaluation The photocatalytic activity of as-prepared catalysts was evaluated by the photodegradation of RhB, a model pollutant. Generally, 150 mL of RhB solution at pH 3 and an initial concentration of 20 mg/L were conducted in photocatalytic procedures, together with 50 mg of catalyst mass (0.3 g/L mass-to-volume ratio). A quartz glass beaker was placed in a temperature-controlled bath at 25 °C, and a 250W Xenon lamp was located 20 cm above the solution surface. At 30-minute intervals during irradiation, by using UV-visible absorption spectroscopy at a wavelength of 554 nm, the RhB concentration was monitored to assess the catalytic activity of the synthesized samples. The total light irradiation time was 120 minutes.

For an experimental test with the effect of CeO_2 content, the ratios calculated by a mass percentage of CeO_2 were chosen as follows: 0%, 0.5%, 1.5%, and 5%.

The influence of RhB initial concentration was conducted at three concentrations: 10, 20, 30, and 40 ppm.

The pH range from 1.5 to 6.3 was chosen to investigate the effect of pH on RhB decomposition efficiency.

The percentage 2,4-D degradation was calculated using the formula:

$$Degradation\ H\% = \frac{(C_o - C_t)}{C_o} \times 100 \quad (1)$$

where C_0 is the initial (at zero minutes) concentration of RhB in solution and C_t is the concentration of RhB after a time interval of t.

3. Results and Discussion

3.1. Characterization of as-synthesized Material

XRD analysis

X-ray diffraction (XRD) patterns of rGO, 0.5CeOx/rGO, 1.5CeOx/rGO, and 5CeOx/rGO were presented in Figure 1.

In the XRD pattern of pure CeO_2, the diffraction peaks with 2θ angles of 28.3°, 32.9°, 47.3°, 56.2°, and 69.8° correspond to the (111), (200), (220), (311), and (400) crystal planes of cubic CeO_2, respectively. This corresponds to the CeO_2 standard pdf card (JCPDS 34-0394) [14-16]. The high intensity and sharp peaks reveal that CeO_2 has high crystallinity. Two distinctive peaks are shown in the XRD pattern of pure rGO at 2θ angles of 24.3°, which is usual for the (002) plane, and 43.1°, which is typical for the (100) plane (JCPDS file no. 75 - 2078) [12].

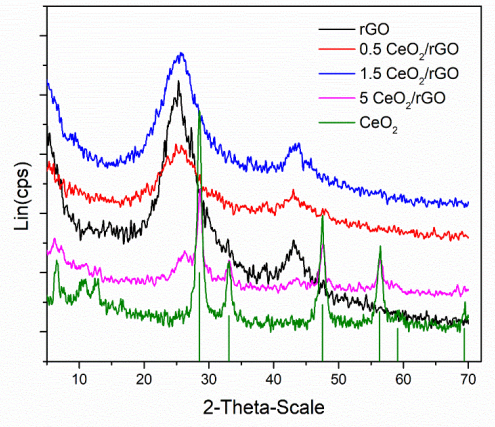

Figure 1. XRD of rGO; 0.5CeOx/rGO; 1.5CeOx/rGO; và 5.0CeOx/Rgo.

The diffraction peaks of pure CeO_2 and pure rGO are visible in the XRD patterns for the CeO_2/rGO sample, indicating the coexistence of these compounds in the composites (2θ angles of 24.3° and 43.1° for rGO and 2θ angles of 28.02, 33, 11, 47.45,

56.33, 59.08, 69.4, 76.69 for CeO_2). When the amount of CeO_2 in the CeO_2/rGO sample increases, the intensity of the characteristic peaks for rGO gradually weakens, while the peaks specific to CeO_2 gradually intensify, indicating a strong interaction between g- CeO_2 and rGO, especially the 5% CeO_2 content. However, these peaks are not seen in samples with low CeO_2 contents, e.g., 0.5% and 1.5%, because of the low CeO_2 content.

EDX analysis

X-ray energy-dispersive spectroscopy was employed to identify the as-synthesized sample's elemental composition.

Figure 2 and Table 1 present the findings.

The EDX spectrum analysis results show that O, with a mass greater than 12.70%, and C, with a loading greater than 83.31%, are the primary components of the rGO.

The findings of the EDX spectrum analysis in Table 1 also show that Ce content in pristine rGO, 0.5%CeOx/rGO, 1.5%CeOx/rGO, and 5%CeOx/rGO were analyzed as follows: 0%, 0.16%, 0.37%, and 1.5%, respectively. Although there are variations from the estimated amounts, these results are entirely consistent with the XRD results' appearance of a distinctive CeO_2 peak. This remarkable concordance could be regarded as evidence that the synthesis procedure is successful. In addition to the main elements, the samples also export some impurities, e.g., Na, Ba, S, and Ni, but the content is quite low. These substances appear to be probably from synthetic precursors. However, for ease of reading, we kept the sample's original symbols.

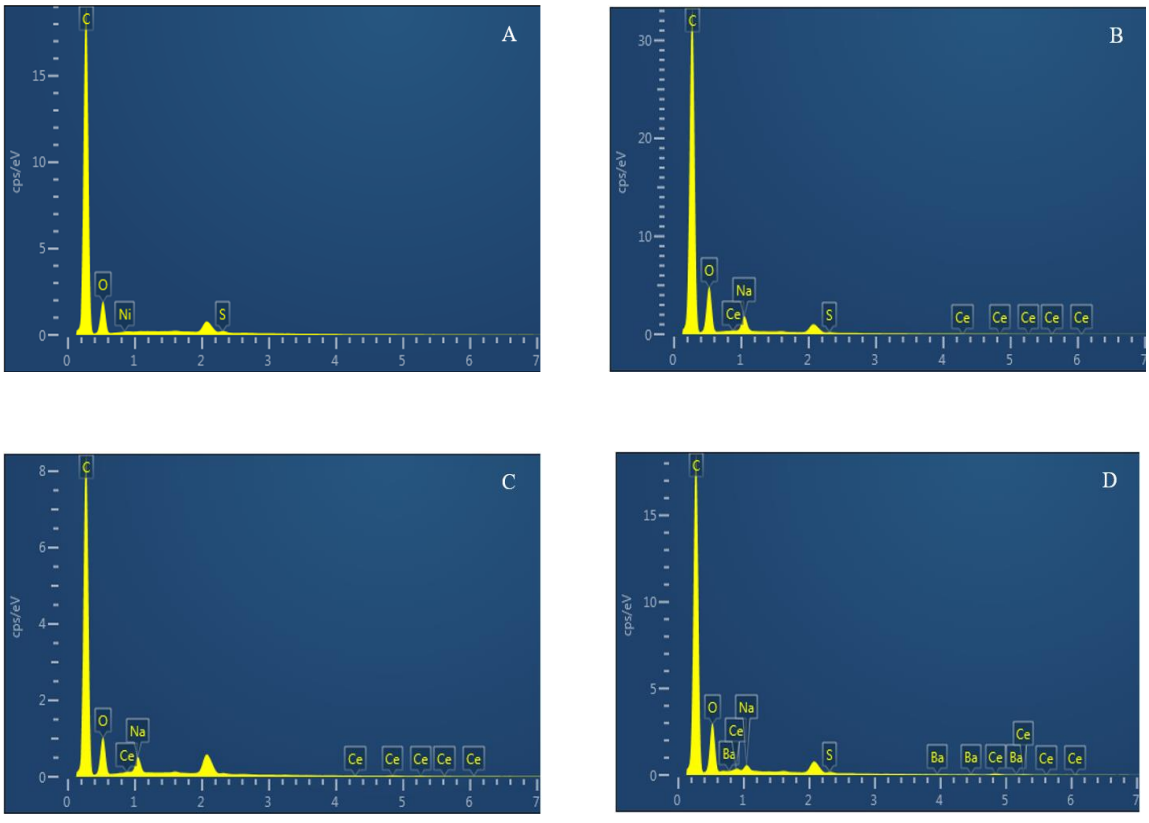

Figure 2. EDX spectrum of rGO (A); 0.5%CeOx/rGO (B); 1.5% CeOx/rGO (C); 5%CeOx/rGO (D).

Table 1. Elemental composition (wt%) of four synthesized materials

Sample	Elemental composition (%)					Total
	C	O	Ce	Na	Impurities	
rGO	87.17	12.70	0.0	0.0	0.13	100
0.5% CeO_x/rGO	83.31	15.54	0.13	1.00	0.02	100
1.5% CeO_x/rGO	85.28	13.33	0.30	1.09	0.0	100
5% CeO_x/rGO	83.54	14.72	1.22	0.39	0.13	100

Figure 3 displays energy dispersive X-ray (EDX) mapping analysis of carbon, oxygen, and cerium atoms for as-prepared samples (rGO, x%CeO_2/rGO (x = 0.5, 1.5, and 5). It is evident from the elemental distribution map that the distribution of elements is fairly uniform. The Ce element is widely distributed throughout the sample surface rather than being concentrated in one area. According to the data, CeO_2 is successfully loaded and uniformly distributed across the surface of rGO.

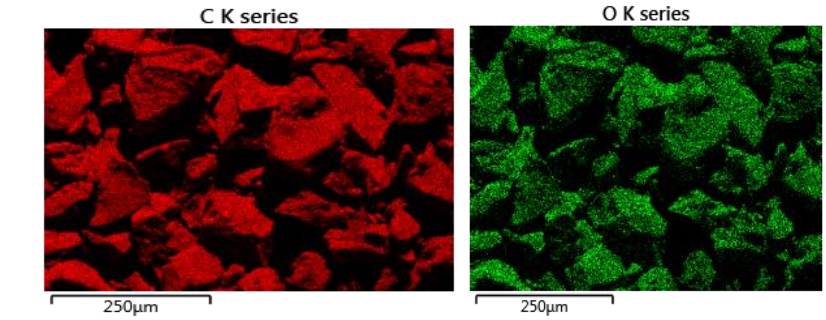

rGO

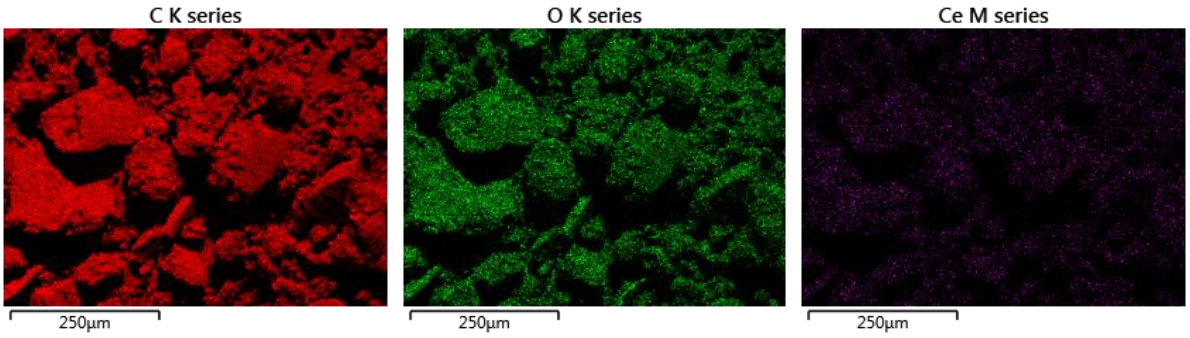

0.5%CeO_2/rGO

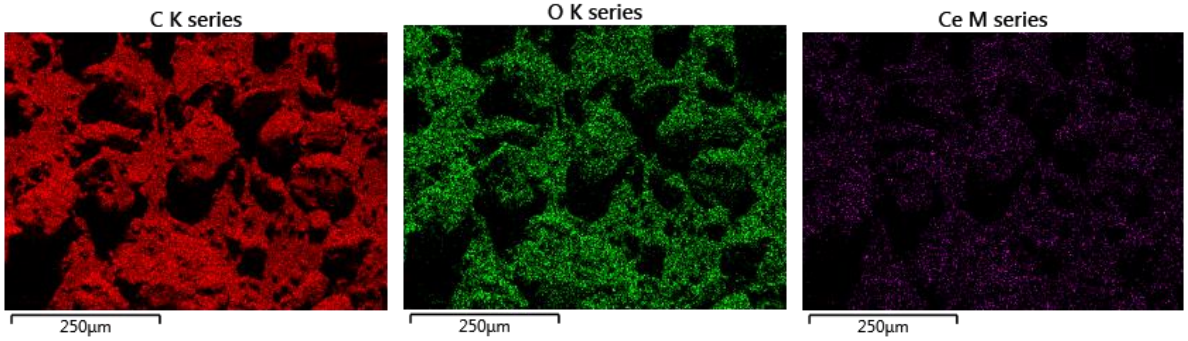

1.5%CeO_2/rGO

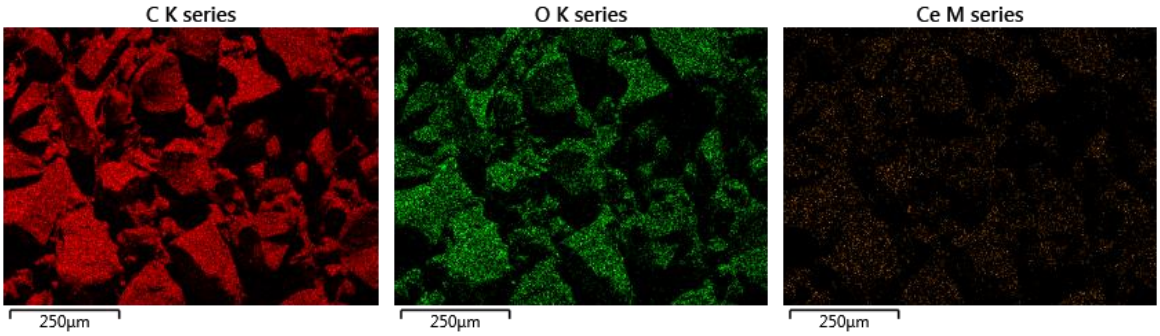

Figure 3. Energy dispersive X-ray (EDX) mapping analysis of carbon, oxygen, and cerium atoms for rGO, 0.5%CeO_2/rGO, 1.5% CeO_2/rGO, and 5%CeO_2/rGO.

FESEM analysis

The morphology of rGO, 0.5%CeO_2/rGO,1.5% CeO_2/rGO, and 5%CeO_2/rGO were evaluated by FeSEM as shown in Figure 4.

From the FeSEM image of rGO (Figure 4A), it can be observed partially folded transparent wave-like nanosheets along with slight fluctuations. In the case of x%CeO_2/rGO (x = 0.5, 1.5, and 5) materials, CeO_2 was aggregated into small clusters and incorporated in the rGO wave-like nanosheets, as seen in Figure 4B, 4C, and 4D. These clusters gradually became bigger as the amount of CeO_2 increased. These proved the formation of a heterojunction between CeO_2 and rGO, which might enhance the materials' ability to separate electrons and holes and the photocatalytic activity of x%CeO_2/rGO materials.

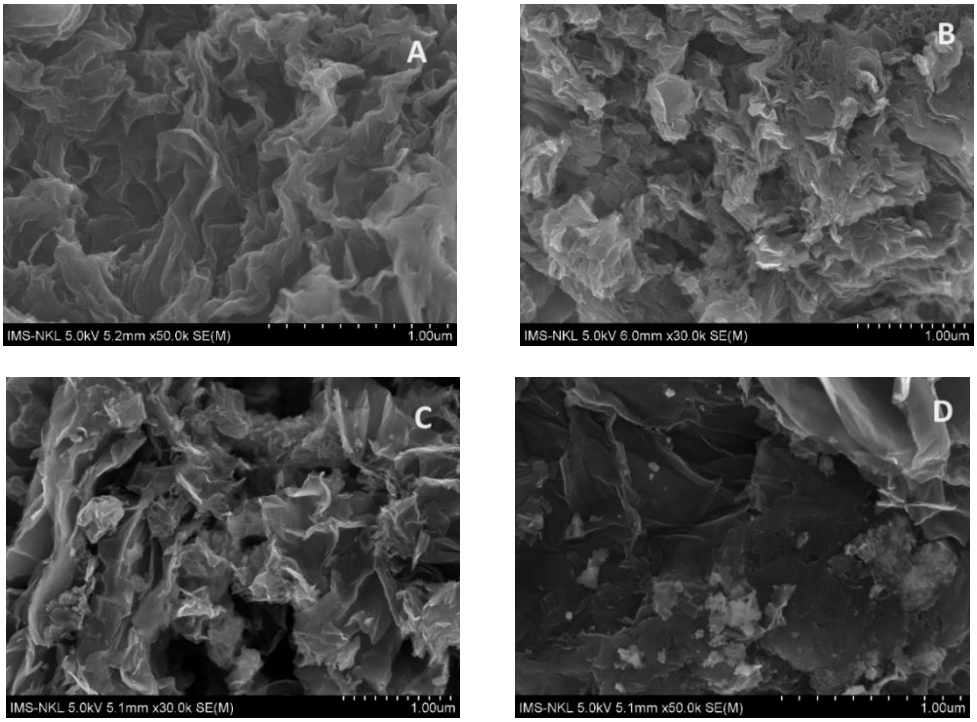

Figure 4. FESEM images of rGO (A), 0.5% CeO_2/rGO (B), 1.5% CeO_2/rGO (C), and 5% CeO_2/rGO (D).

UV Vis DRS analysis

The UV-Vis diffuse reflectance spectra of rGO and x%CeO_2/rGO (x = 0.5, 1.5, and 5) materials are displayed in Figure 5.

According to the UV-Vis diagram, the pure CeO_2 sample possessed a high optical absorption at low 400 nm, whereas rGO exhibited lower light absorption intensity at a wavelength of around 360 nm. In comparison to rGO, x%CeO_2/rGO materials (x = 0.5, 1.5, and 5) showed intensive light absorption capability, which could be attributed to the interaction between rGO and CeO_2. The 1.5%CeO_2/rGO materials exhibit the highest intensity of light absorption.

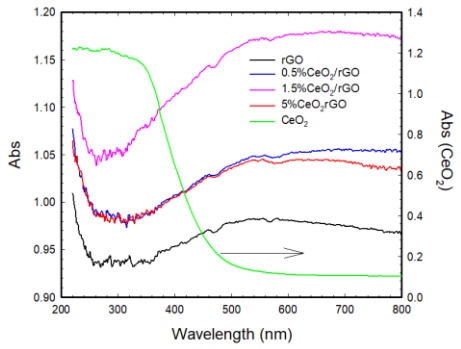

Figure 5. UV vis DRS spectra of rGO and x%CeO_2/rGO (x = 0.5, 1.5 and 5).

3.2. Photocatalytic Activity

The effect of CeO_2 loading on the conversion of RhB under light irradiation.

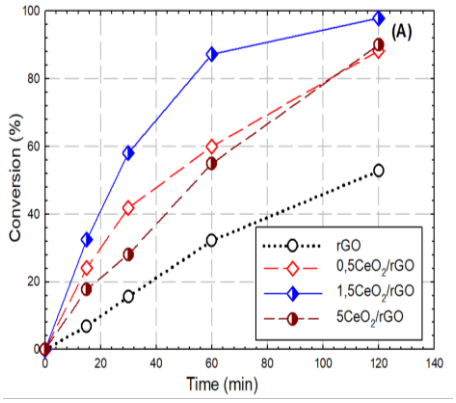

Figure 6. Effect of CeO_2 loading on conversion of RhB under light irradiation.

The loading of catalytic centers in the x%CeO_2/rGO sample will vary depending on the CeO_2 content, which will directly impact the oxidation ability of the material. Three CeO_2 loadings, such as 0.5; 1.5; and 5% by weight, were investigated to evaluate the effect of CeO_2 loading on the photocatalytic activity of the as-prepared materials for the removal of RhB dye. The findings are displayed in Figure 6.

From Figure 6, it can be seen that the RhB degradation efficiency of CeO_2/rGO gradually increased with increasing lighting time. At 60 minutes of illumination, the RhB degradation efficiency reached about 36%, 60%, 85%, and 55% for rGO, 0.5%CeO_2/rGO, 1.5%CeO_2/rGO, and 5%CeO_2/rGO respectively. The highest RhB degradation efficiency reached 52%, 84%, 98.8%, and 86% for rGO, 0.5%CeO_2/rGO, 1.5%CeO_2/rGO, and 5%CeO_2/rGO after 120 minutes of illumination. On the other hand, the findings also indicate that the RhB degradation conversation increased noticeably when the CeO_2 loading in the CeO_2/rGO sample increased from 0.5% to 1.5% under the same conditions. However, the RhB degradation starts to decline as the CeO_2 loading is raised up to 5% (denoted as 5%CeO_2/rGO). The results can be explained by the shrinkage of the CeO_2 center clusters, which reduces dispersion when increasing the CeO_2 content to 5% and is completely consistent with the results characterized by the FeSEM image when the CeO_2 clusters at a loading of 5% are quite large.

Consequently, photocatalytic performance is arranged in the following order: rGO < 5%CeO_2/rGO < 0.5%CeO_2/rGO < 1.5%CeO_2/rGO. Based on these findings, the material 1.5%CeO_2/rGO was chosen for additional study.

Table 2 show the comparison of the RhB photodegradation efficiency of published catalysts.

From this comparison result, it is seen that 1.5%CeO_2/rGO material also exhibits strong photocatalytic activity for RhB decomposition under light irradiation.

Table 2. Comparison of performance of different photocatalysts

Catalysts	Amount Cat.	RhB initial amount	Power	Irradiation time	H%	Reference
RGO/Ag	20 mg	100 mL (1mg/L) = 0.1 mg	Visible light	80 min	85	[17]
Ag_2O/g-C_3N_4-Fe_2O_3	10 mg	20 mL (10 mg/L) = 0.2 mg	500 W Xenon lamp	60 min	98.3	[18]
8% SiC/g-C_3N_4	20 mg	80 mL (20 mg/L) = 1.6 mg	300 W Xenon lamp	150 min	65	[19]
10% Ag_3PO_4/$NTiO_2$	20 mg	10 mg/L	150 W Xenon lamp	120 min	99	[20]
20%$LaFeO_3$/g-C_3N_4	20 mg	100 Ml (15 mg/L)	A 500 W Xe arc lamp	160 min	97	[21]
N-doped MoS_2	20 mg	50 ml (30 mg/L) =1.5 mg	175 W halogen lamp	70 min	99	[22]
Gelatin/CuS/PVA	20 mg	50 mL (50mg/L) = 2.5 mg	solar light	80 min	96	[23]
1.5%CeO_2/rGO	50 mg	150 mL (20 mg/L) = 3 mg	250 W xenon lamp	120 min	92.8	This work

The effect of initial concentration of RhB on RhB degradation efficiency under light irradiation.

RhB solutions with varying initial concentrations (10, 20, 30, and 40 mg/L) were used in the study. The illumination time is 120 minutes. The mass ratio of the material to the volume of the RhB solution was 0.3 g/L. The obtained results are shown in Figure 7.

It is evident from Figure 7 that the RhB degradation conversion decreased with increasing the initial concentration of RhB. Specifically, RhB degradation efficiency diminished from 92.32% to 8.53% as RhB concentrations increased from 10 mg/L to 40 mg/L after 60 minutes of illumination. Moreover, the degradation of RhB is over 85.0% at all studied concentrations after 120 minutes. In particular, for the initial concentration of 10 mg/L, RhB is completely degraded within 90 minutes.

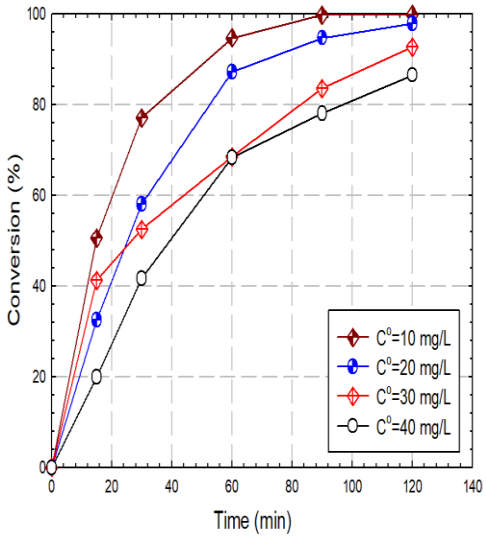

Figure 7. Effect of initial concentration of RhB (10, 20, 30, and 40 mg/L) on RhB degradation efficiency under light irradiation.

With concentrations of 30 and 40 mg/L, at 120 minutes, the conversion efficiency is 92.70 and 86.53%, respectively, meaning the RhB dye had not been completely processed at this time. A concentration of 20 mg/L at this period had a conversion of 97.80%, which could be considered almost complete. As a result, in the experiments that follow, a concentration of 20 mg/L was utilized to examine the material's efficiency.

The effect of pH on RhB degradation conversion under light irradiation.

To investigate the effect of pH, RhodaminB degradation experiments were conducted at different pHs, changing pH values from 1.5 to 6.3. The results of the influence of pH are presented in Figure 8.

As shown in Figure 8, the RhB degradation over 1.5%CeO_2/rGO material varied quite quickly with the change in pH value during 120-minute irradiation. The findings indicate that RhB was well decomposed at low pH. Respectively, RhB degradation conversion reached 98.9% at pH 1.5 after 60 minutes of lighting, while at pH 2.5, RhB decomposition efficiency reached 87.21% and at pH 3, RhB degradation efficiency reached 73.29%. As pH continues to increase to pH 4.8 and pH 6.3, the RhB decomposition efficiency will continue to decrease by 55.82% and 46.21% at the same lighting time.

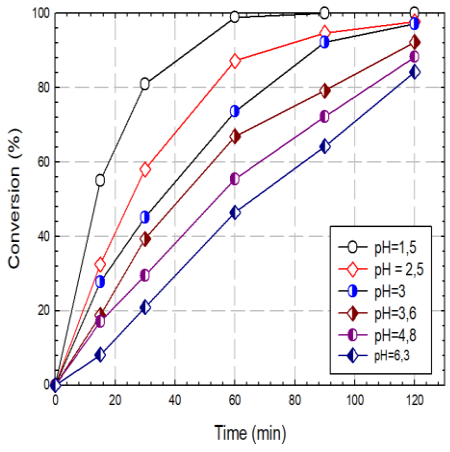

Figure 8. Efferent of pH on RhB degradation conversion under light irradiation.

After 120 minutes, RhB decomposition efficiency did not much change, with a conversion of about 100% when increasing pH from 1.5 to 3. However, RhB decomposition efficiency continues to increase significantly as pH changes from 3.6 to 6.3 at the same irradiation time. For example, 82.03% and 84.11% RhB were decomposed at pHs of 4.8 and 6.3, respectively.

According to [24], at pH below 4.0, the following chain reactions are initiated that produce more $^{\bullet}O_2^-$ and $^{\bullet}OH$ free radicals:

$$^{\bullet}O_2^- + H^+ \rightleftharpoons HO_2^{\bullet}$$
$$2HO_2^{\bullet} \rightarrow O_2 + H_2O_2$$
$$HO_2^{\bullet} + {}^{\bullet}O_2^- \rightarrow HO_2^- + O_2$$
$$HO_2^- + H^+ \rightarrow H_2O_2$$
$$H_2O_2 + e^- \rightarrow {}^{\bullet}H_2O_2$$
$$^{\bullet}H_2O_2 + {}^{\bullet}O_2^- \rightarrow {}^{\bullet}OH + OH^- + O_2$$
$$H_2O_2 \xrightarrow{h\nu} 2\ {}^{\bullet}OH$$

The mechanism of photocatalytic degradation is known to involve both h^+ holes and $^{\bullet}OH$, $^{\bullet}O_2^-$ free radicals, with both playing equivalent roles [24]. Therefore, it can be explained that a low pH is favorable for the decomposition of RhB by free radicals. Through the results of this survey, a low pH of 3 was chosen for this study.

Theoretically, a hypothesis regarding the RhB degradation mechanism can be proposed as follows: Under the influence of illumination with an appropriate wavelength, electrons in the catalyst are excited from the valence band (VB) to the conduction band (CB). In the CB, photo-generated electrons react with dissolved oxygen in the water (reduction reaction) to create superoxide radicals. These radicals continue a chain reaction to form H_2O_2 under low pH conditions, which then produces OH radicals. In the VB, photo-generated holes oxidize water to create OH radicals. The generated radicals (superoxide, OH radicals, and photo-generated holes) participate in the degradation of RhB.

4. Conclusion

EDX, XRD, FeSEM, and UV-Vis DRS were used to characterize the as-synthesized materials. For RhB degradation, the 1.5%CeO_2/rGO showed the best photocatalytic activity. The degradation efficiency of RhB with an initial concentration of 20 mg/L was about 100% after 120 minutes of illumination. The mass ratio of the material to the volume of the RhB solution is 0.3 g/L and the pH solution of RhB was 3.

Acknowledgements

This work is funded by the Ministry of Science and Technology under grant no. B2022-TDV-06.

Conflict of Interest

The authors declare that they have no conflicts of interest.

References

[1] Saravanan, P. S. Kumar, R. V. Hemavathy, S. Jeevanantham, P. Harikumar, G. Priyanka, D. R. A. Devakirubai, A Comprehensive Review on Sources, Analysis and Toxicity of Environmental Pollutants and its Removal Methods from Water Environment, Science of the Total Environment, Vol. 812, 2022, pp. 152456, https://doi.org/10.1016/j.scitotenv.2021.152456.

[2] A. Nishat, M. Yusuf, A. Qadir, Y. Ezaier, V. Vambol, M. I. Khan, S. B. Moussa, H. Kamyab, S. S. Sehgal, C. Prakash, H. H. Yang, H. Ibrahim, S. M. Eldin, Wastewater Treatment: A Short Assessment on Available Techniques, Alexandria Engineering Journal, Vol. 76, 2023, pp. 505-516, https://doi.org/10.1016/j.aej.2023.06.054.

[3] A. Saravanan, P. S. Kumar, S. Jeevanantham, S. Karishma, B. Tajsabreen, P. R. Yaashikaa, B. Reshma, Effective Water/wastewater Treatment Methodologies for Toxic Pollutants Removal: Processes and Applications Towards Sustainable Development, Chemosphere, Vol. 280, 2021, pp. 130595, https://doi.org/10.1016/j.chemosphere.2021.130595.

[4] G. Ren, H. Han, Y. Wang, S. Liu, J. Zhao, X. Meng, Z. Li, Recent Advances of Photocatalytic Application in Water Treatment: A Review. Nanomaterials Vol. 11, No. 7, 2021, pp. 1804, https://doi.org/10.3390/nano11071804.

[5] A. A. Fauzi, A. A. Jalil, N. S. Hassan, F. F. A. Aziz, M. S. Azami, I. Hussain, R. Saravanan, D. V. N. Vo, A Critical Review on Relationship of CeO_2-based Photocatalyst Towards Mechanistic Degradation of Organic Pollutant, Chemosphere, Vol. 286, Part 1, 2022, pp. 131651, https://doi.org/10.1016/j.chemosphere.2021.131651.

[6] J. Yao, Z. Gao, Q. Meng, G. He, H. Chen, One-Step Synthesis of Reduced Graphene Oxide Based Ceric Dioxide Modified with Cadmium Sulfide (CeO_2/CdS/RGO) Heterojunction With Enhanced Sunlight-driven Photocatalytic Activity, Journal of Colloid and Interface Science, Vol. 594, 2021, pp. 621-634, https://doi.org/10.1016/j.jcis.2021.03.034.

[7] B. Sun, W. Chen, W. Zheng, H. Zhang, T. X. Liu, A. Elmarakbi, Y. Q. Fu, In-situ Controlled Growth of Ultrafine CeO_2 Nanoparticles on Reduced Graphene Oxides for Efficient Photocatalytic Degradation, Journal of Catalysis, Vol. 424, 2023, pp. 106-120, https://doi.org/10.1016/j.jcat.2023.05.014.

[8] M. T. Qamar, S. Iqbal, M. Aslam, A. Alhujaily, A. Bilal, K. Rizwan, H. M. U. Farooq, T. A. Sheikh, A. Bahadur, N. S. Awwad, H. A. Ibrahium, R. S. Almufarij, E. B. Elkaeed, Transition Metal Doped CeO_2 for Photocatalytic Removal of 2- Chlorophenol in the Exposure of Indoor White Light and Antifungal Activity, Front. Chem, Vol. 11, 2023, pp. 1126171, https://doi.org/10.3389/fchem.2023.1126171.

[9] H. Yan, N. Zhang, D. Wang, Highly Efficient CeO_2-Supported Noble-metal Catalysts: From Single Atoms to Nanoclusters, Chem Catalysis, Vol. 2, Issue 7, 2022, pp. 1594-1623, https://doi.org/10.1016/j.checat.2022.05.001.

[10] W. Fan, Q. Zhang, Y. Wang, Semiconductor-Based Nanocomposites for Photocatalytic H_2 Production and CO_2 Conversion, Phys. Chem. Chem. Phys, Vol. 15, 2013, pp. 2632-2649, https://doi.org/10.1039/c2cp43524a.

[11] D. Zhu, Z. Dong, F. Lv, C. Zhong, W. Huang, The Development of Balanced Heterojunction Photocatalysts, Cell Reports Physical Science, Vol. 3, Issue 10, 2022, pp. 101082, https://doi.org/10.1016/j.xcrp.2022.101082.

[12] B. Gupta, N. Kumar, K. Panda, Role of Oxygen Functional Groups in Reduced Graphene Oxide for Lubrication. Sci Rep. Vol. 7, 2017, pp. 45030, https://doi.org/10.1038/srep45030.

[13] Aziz, A. F. Ismail, M. H. D. Othman, M. A. Rahman, F. Aziz, N. Yusof, R. Mohamud, Tuning the Oxygen Functional Groups in Graphene Oxide Nanosheets by Optimizing the Oxidation Time, Physica E: Low-dimensional Systems and Nanostructures, Vol. 131, 2021, pp. 114727, https://doi.org/10.1016/j.physe.2021.114727.

[14] M. A. Abbasi, K. M. Amin, M. Ali, Z. Ali, M. Atif, W. Ensinger, W. Khalid, Synergetic Effect of Adsorption-Photocatalysis by GO−CeO_2 Nanocomposites for Photodegradation of Doxorubicin, Journal of Environmental Chemical Engineering, Vol. 10, Issue 1, 2022, pp. 107078, https://doi.org/10.1016/j.jece.2021.107078.

[15] F. Nemati, M. Rezaie, H. Tabesh, K. Eid, G. Xu, M. R. Ganjali, M. Hosseini, C. Karaman, N. Erk, P. L. Show, N. Zare, H. K. Maleh, Cerium Functionalized Graphene Nano-Structures and Their Applications; A Review, Environmental Research, Vol. 208, 2022, pp. 112685, https://doi.org/10.1016/j.envres.2022.112685.

[16] A. Murali, Y. P. Lan, P. K. Sarswat, M. L. Free, Synthesis of CeO_2/Reduced Graphene Oxide Nanocomposite for Electrochemical Determination of Ascorbic Acid and Dopamine and for Photocatalytic Applications, Materials Today Chemistry, Vol. 12, 2019, pp. 222-232, https://doi.org/10.1016/j.mtchem.2019.02.001.

[17] R. Liu, Y. Liu, C. Liu, S. Luo, Y. Teng, L. Yang, R. Yang, Q. Cai, Enhanced Photoelectrocatalytic Degradation of 2,4-Dichlorophenoxyacetic Acid by $CuInS_2$ Nanoparticles Deposition onto TiO_2 Nanotube Arrays, J. Alloys Compd, Vol. 509, Issue 5, 2011, pp. 2434-2440, https://doi.org/10.1016/j.jallcom.2010.11.040.

[18] K. S. Divya, A. Chandran, V. N. Reethu, S. Mathew, Enhanced Photocatalytic Performance of RGO/Ag Nanocomposites Produced via a Facile Microwave Irradiation for the Degradation of Rhodamine B in Aqueous Solution, Applied Surface Science, Vol. 444, 2018, pp. 811-818, https://doi.org/10.1016/j.apsusc.2018.01.303.

[19] D. Zhang, S. Cui, J. Yang, Preparation of Ag_2O/g-C_3N_4/ Fe_3O_4 Composites and the Application in the Photocatalytic Degradation of Rhodamine B Under Visible Light, Journal of Alloys and Compounds, Vol. 708, 2017, pp. 1141-1149, https://doi.org/10.1016/j.jallcom.2017.03.095.

[20] F. Chang, J. Zheng, X. Wang, Q. Xua, B. Deng, X. Hu, X. Liu, Heterojuncted Non-Metal Binary Composites Silicon Carbide/g-C3N4 with Enhanced Photocatalytic Performance, Materials Science in Semiconductor Processing, Vol. 75, 2018, pp. 183-192, https://doi.org/10.1016/j.mssp.2017.11.043.

[21] N. R. Khalid, U. Mazia, M. B. Tahir, N. A. Niaz, M. A. Javid, Photocatalytic Degradation of RhB from an Aqueous Solution Using Ag_3PO_4/N-TiO_2 Heterostructure, Journal of Molecular Liquids, Vol. 313, 2020, pp. 113522, https://doi.org/10.1016/j.molliq.2020.113522.

[22] Q. Liang, J. Jin, C. Liu, S. Xu, Z. Li, Constructing a Novel p-n Heterojunction Photocatalyst $LaFeO_3$/g-C_3N_4 with Enhanced Visible-light-Driven Photocatalytic Activity, Journal of Alloys and Compounds, Vol. 709, 2017, pp. 542-548, https://doi.org/10.1016/j.jallcom.2017.03.190.

[23] P. Liu, Y. Liu, W. Ye, J. Ma, D. Gao, Flower-like N-doped MoS_2 for Photocatalytic Degradation of RhB by Visible Light Irradiation, Nanotechnology, Vol. 27, 2016, pp. 225403-225410, https://doi.org/10.1088/0957-4484/27/22/225403.

[24] A. A. Kahtani, Photocatalytic Degradation of Rhodamine B Dye in Wastewater Using Gelatin/CuS/PVA Nanocomposites under Solar Light Irradiation, Journal of Biomaterials and Nanobiotechnology, Vol. 8, 2017, pp. 66-82, https//doi.org/10.4236/jbnb.2017.81005.

[25] R. Liu, Y. Liu, C. Liu, S. Luo, Y. Teng, L. Yang, R. Yang, Q. Cai, Enhanced Photoelectrocatalytic Degradation of 2,4-Dichlorophenoxyacetic Acid by $CuInS_2$ Nanoparticles Deposition onto TiO_2 Nanotube Arrays,Journal of Alloys and Compounds, Vol. 509, Issue 5, 2011, pp. 2434-2440, https://doi.org/10.1016/j.jallcom.2010.11.040.